The Journal of Engineering

IET International Radar Conference (IRC 2018)

IET Journals
The Institution of Engineering and Technology

WiFi-based imaging for ground penetrating radar applications: fundamental study and experimental results

eISSN 2051-3305
Received on 19th February 2019
Accepted on 2nd May 2019
doi: 10.1049/joe.2019.0209
www.ietdl.org

Weike Feng[1] ✉, Jean-Michel Friedt[2], Zhipeng Hu[3], Grigory Cherniak[1], Motoyuki Sato[4]

[1]*Graduate School of Environmental Studies, Tohoku University, Sendai, Japan*
[2]*Time & Frequency department, FEMTO-ST, Besancon, France*
[3]*College of Geoexploration Science and Technology, Jilin University, Changchun, People's Republic of China*
[4]*Center for Northeast Asian Studies, Tohoku University, Sendai, Japan*
✉ *E-mail: feng.weike.q4@dc.tohoku.ac.jp*

Abstract: As a fundamental research step for subsurface target imaging by passive ground penetrating radar, some simulation and experimental results of passive bistatic radar imaging for short-range targets by using IEEE 802.11 Wireless Fidelity (WiFi) wave as the source of illumination have been presented. As the WiFi signal only penetrates shallow layers and yet lacks bandwidth for high resolution subsurface structure mapping, the interrogation of cooperative targets with the passive bistatic radar approach is demonstrated. This strategy is achieved by inserting surface acoustic wave (SAW) delay lines acting as dedicated reflectors allowing for subsurface tagging (identification) or sensing (temperature measurement) through the fine measurement of echo delays. Experimental results show that short-range targets, such as cars and metallic plates located within 10 m, can effectively be detected and imaged. The response of the SAW delay lines can also be well probed.

1 Introduction

Ground penetrating radar (GPR) is a safe and cost-effective tool for subsurface exploration. It works by transmitting electromagnetic waves into subsurface and receiving the reflected waves to acquire various information of the subsurface feature. The depth, size, shape and other parameters of the subsurface reflectors can be derived. Therefore, GPR has been used for many applications, such as cultural-heritage management, humanitarian demining, civil engineering etc. [1, 2].

A GPR system is composed of three main components, which includes transmitter, receiver, and control unit. Due to the regulation limitation, the transmitters of most GPR systems should be placed close to the ground surface to avoid generating additional electromagnetic pollution to the environment. To overcome this limitation, in our research, non-cooperative transmitters, such as digital terrestrial television broadcasting signal, global system for mobile communications (GSM) signal, and IEEE 802.11 Wireless Fidelity (WiFi) signal, are considered to be the source of illumination to replace the dedicated transmitter of GPR [3, 4]. Unlike active radar, using existing non-cooperative sources is advantageous since there is no requirement of the specific frequency allocation.

In this paper, we present some simulation and experimental results of WiFi-based passive bistatic radar imaging for GPR applications. Although WiFi signal based range–Doppler mapping, through-the-wall imaging, and object localisation have been well addressed in the last decade [5–9], we show some different considerations specific to subsurface target mapping. WiFi waves with IEEE 802.11n standard, 2.4 GHz frequency, and 40 MHz bandwidth and WiFi waves with IEEE 802.11 ac standard, 5 GHz frequency, and 80 MHz bandwidth are employed for short-range target imaging by using synthetic aperture radar (SAR) technique [10–12]. It is noticed that, in [9], high-resolution SAR imaging with IEEE 802.11 ac signal with 160 MHz bandwidth has been studied by numerical simulations. However, we show the practical implementations of WiFi radar imaging in this paper. Being aware of the fact that the range solution is insufficient for GPR subsurface shallow target imaging (such as concrete monitoring), a passive and wireless cooperative sensor designed by surface acoustic wave (SAW) delay lines [13] is also tested. Our experiments show that cars and metallic plates located within 10 m can be effectively detected and imaged. The response of the SAW delay lines is probed at a bistatic range of up to 1.5 m and allows recovering the identity as well as temperature of the sensor.

2 WiFi-based bistatic SAR imaging

2.1 Signal model

In this subsection, the signal model for WiFi-based bistatic SAR imaging is established. Since the WiFi transmitter is always stationary, in order to achieve high azimuth resolution, a measurement antenna is assumed to be moved linearly to form a synthetic aperture. Normally, the non-cooperative transmitted signal cannot directly be obtained. Therefore, a reference antenna is required to sample the reference signal for cross-correlation based range compression. When the measurement antenna is at the lth position $(x_l, 0)$, without considering the multipath echoes in the reference channel, the received reference signal and the measurement signal can be expressed as

$$s_{\mathrm{ref}}^{l}(t) = A_{\mathrm{ref}}^{l} s_0(t - t_{\mathrm{ref}}) + n_{\mathrm{ref}}^{l}(t) \tag{1}$$

and

$$s_{\mathrm{sur}}^{l}(t) = s_{\mathrm{dirc}}^{l}(t) + \sum_{i=1}^{I} \alpha_i s_0(t - t_i^{l}) + n_{\mathrm{sur}}^{l}(t), \tag{2}$$

where t_{ref} is the time delay between the reference antenna and the WiFi transmitter, which is constant for $l = 1,\ldots, N$, and $s_{\mathrm{dirc}}^{l}(t) = A_{\mathrm{sur}}^{l} s_0(t - t_{\mathrm{sur}}^{l})$ is the direct-path signal received by the measurement antenna, α_i is the reflection coefficient of the ith target, $i = 1,2,\ldots, I$, I is the number of targets, and t_i^{l} is the time delay of ith target from the WiFi transmitter to the measurement antenna at the lth position.

In practice, the direct-path signal is much stronger than the echoes of the targets. In this paper, we use the extensive cancellation algorithm (ECA) [14] to suppress its influences. For the lth position of measurement antenna, the refined measurement signal is given by

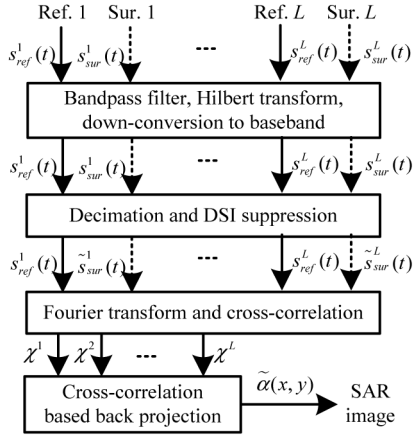

Fig. 1 *Signal processing chain for WiFi-based passive SAR imaging*

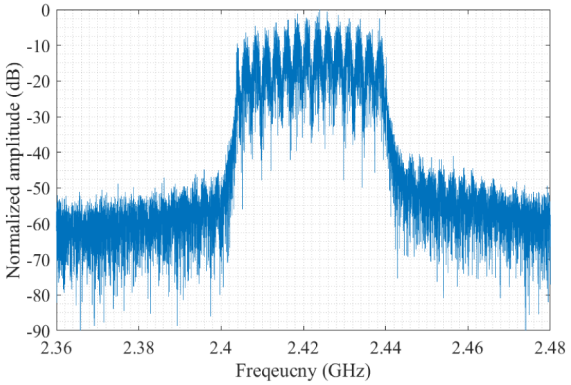

Fig. 2 *Spectrum of real IEEE 802.11n signal with 40 MHz bandwidth used in the simulations*

$$s_{\text{sur}}^{\sim l}(t) = (\boldsymbol{I} - \boldsymbol{P}\boldsymbol{P}^{\dagger}) s_{\text{sur}}^{l}(t), \tag{3}$$

where $\boldsymbol{I}$ denotes an identity matrix, $(\cdot)^{\dagger}$ denotes the pseudo-inversion, and $\boldsymbol{P}$ is a matrix formed by the delayed copies of the reference signal $s_{\text{ref}}^{l}(t)$, i.e.

$$\boldsymbol{P} = \begin{bmatrix} s_{\text{ref}}^{l}(0) & 0 & \cdots & 0 \\ s_{\text{ref}}^{l}(1) & s_{\text{ref}}^{l}(0) & \cdots & 0 \\ \vdots & \vdots & \ddots & \vdots \\ s_{\text{ref}}^{l}(N-1) & s_{\text{ref}}^{l}(N-2) & \cdots & s_{\text{ref}}^{l}(N-M) \end{bmatrix}, \tag{4}$$

where M is the number of time delays to properly model the maximum range of the direct-path signal.

Then, the lth range-compressed profile can be obtained by the cross-correlation process as

$$\chi^{l}(\tau) = \int_{0}^{T_{\text{int}}} s_{\text{sur}}^{\sim l}(t) \left[s_{\text{ref}}^{l}(t-\tau) \right]^{*} \mathrm{d}t, \tag{5}$$

where T_{int} denotes the integration time that determines the system signal to noise ratio and the Doppler resolution.

At last, by using back projection (BP) algorithm, the reflection coefficients of targets can be estimated by

$$\tilde{\alpha}(x,y) = \sum_{l=1}^{L} \chi^{l}\left(\frac{\sqrt{(x_l - x)^2 + (y_l - y)^2} + R_{\text{AP}}(x,y)}{c} - t_{\text{ref}} \right), \tag{6}$$

where $R_{\text{AP}}(x,y) = \sqrt{(x_{\text{AP}} - x)^2 + (y_{\text{AP}} - y)^2}$ is the distance between the target and the WiFi transmitter, and $\tilde{\alpha}(x,y)$ is the estimated amplitude of the target at (x,y).

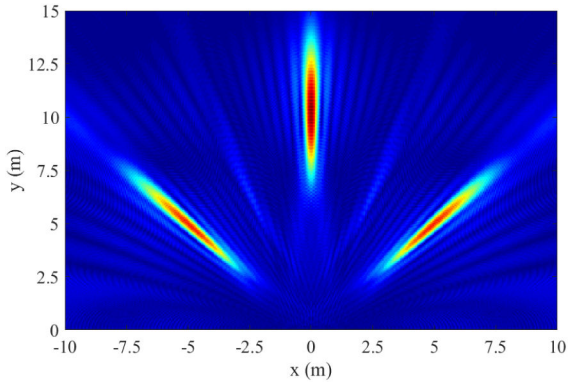

Fig. 3 *Imaging result of three targets obtained by the BP algorithm*

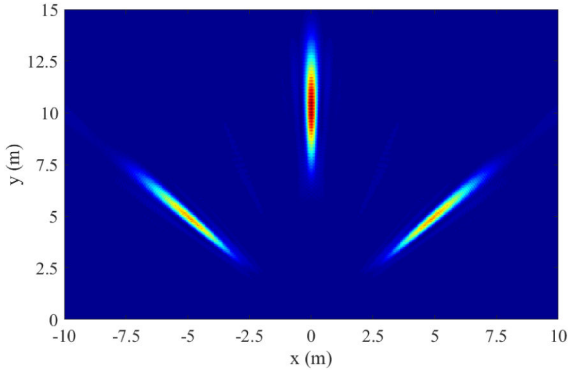

Fig. 4 *Imaging result of three targets obtained by the cross-correlation based BP algorithm*

To suppress the sidelobes caused by the coherent summation of the range-compressed signal from all the antenna positions, the cross-correlation based BP algorithm [15] is further applied, which can be expressed as

$$\tilde{\alpha}(x,y) = \sum_{l_1=1}^{L-1} \sum_{l_2=l_1}^{L} \boldsymbol{\alpha}_{l_1}(x,y) \boldsymbol{\alpha}_{l_2}(x,y), \tag{7}$$

where $\boldsymbol{\alpha}_{l_o}(x,y) = \chi^{l_o}(\tau_{x,y})$, and $o = 1, 2$.

In summary, the signal processing chain for passive bistatic WiFi SAR imaging is presented in Fig. 1.

In order to test the established signal model and the proposed WiFi-based bistatic SAR imaging method, several semi-experiment simulations are conducted. In the simulation, the reference signal is obtained by directly sampling the IEEE 802.11n signal with 40 MHz bandwidth from a WiFi access point (AP), whose spectrum is shown in Fig. 2. The measurement signal at each position is generated by delaying the reference signal with corresponding distance. The synthetic aperture length is simulated to 3 m and three targets located at (0, 10), (−5, 5) and (5, 5) are simulated. The imaging results obtained by the BP algorithm and the cross-correlation based BP algorithm are shown in Figs. 3 and 4, respectively. It can be observed that these three targets can be well focused by both algorithms. However, the sidelobes are much reduced by the cross-correlation based BP algorithm. Therefore, in the practical implementation, the cross-correlation based BP algorithm is used.

2.2 Experimental result

Two experiments are further conducted to validate the WiFi-based bistatic SAR imaging technique. The diagram of the designed system used in the experiments is shown in Fig. 5. The system mainly includes an oscilloscope, a positioner, a WiFi AP used to transmit the signal, two horn antennas, and two PCs that communicate with each other by sending a big file. One PC is used to remotely control the positioner and oscilloscope and process the received data. A horn antenna is facing to the AP and provides the

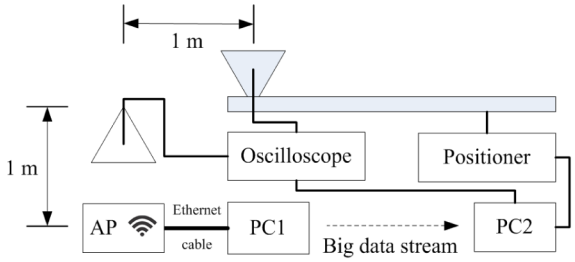

Fig. 5 *Configuration of the designed WiFi-based bistatic SAR system*

Fig. 6 *Experiment setup for passive bistatic SAR imaging*

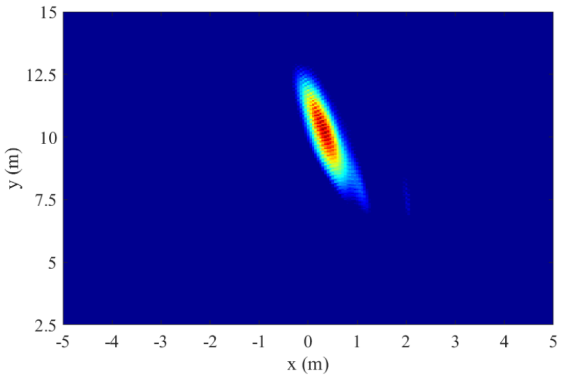

Fig. 7 *Imaging result of the car using IEEE 802.11n signal with 40 MHz bandwidth*

reference signal, and the second horn antenna is sled on the positioner and faced to the target to provide the measurement signal.

In the first experiment, an IEEE 802.11n signal with 40 MHz bandwidth is used to image a car at a distance of about 9 m. The AP is located at (0, −1), the reference antenna is located at (0, 0), and the measurement antenna is sled on the rail from (1, 0) to (4, 0) steps with 5 cm. The data sampling frequency of the oscilloscope is set to 10 GSamples/s and the integration time is about 1.6 μs. The experiment set up is shown in Fig. 6, where the metallic plate is not added in this experiment. With cross-correlation based BP algorithm, the imaging result is shown in Fig. 7. It can be seen that the car can be well focused with correct distance and azimuth, yet with a range resolution 3.75 m limited by the available bandwidth.

In the second experiment, an IEEE 802.11ac signal with 80 MHz bandwidth is applied to increase the range solution of the designed passive bistatic radar system. In such a case, due to the higher signal frequency (5 GHz), the data sampling frequency of the oscilloscope and the integration time are changed to 20 GSamples/s and 0.8 μs, respectively. Besides, the moving step of the measurement antenna is reduced to 2 cm to avoid aliasing. Apart from the car, a metallic plate is added as an additional target. The imaging result is shown in Fig. 8, where the car and plate can be effectively imaged and separated. Compared to the result in Fig. 7, more details of the car can be observed, the range solution is also increased. Furthermore, some parts of a wall can also be imaged in this experiment.

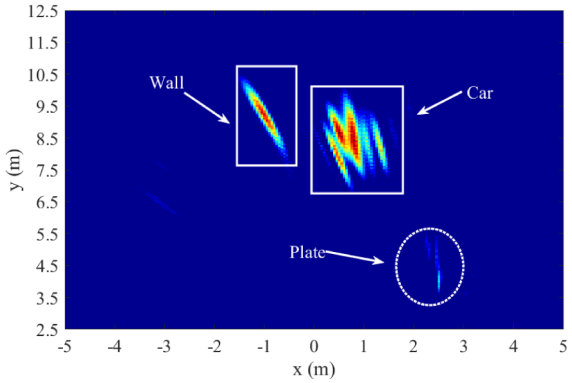

Fig. 8 *Imaging result of the car and metallic plate using IEEE 802.11ac signal with 80 MHz bandwidth*

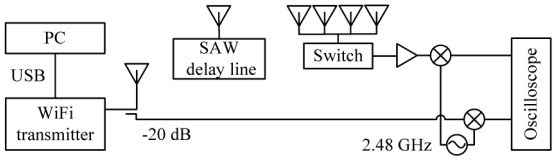

Fig. 9 *Configuration of WiFi-based passive sensor detection*

Fig. 10 *Experiment setup for WiFi-based passive sensor detection*

3 Detection of passive SAW sensors

It can be learned from the previous results shown in Section 2 that, although the short-range targets (car and plate) can be effectively detected and imaged, the limited range resolution caused by the limited bandwidth of the WiFi signal is the main obstacle met for using WiFi-based GPR in the practical mapping of shallow targets such as the underground gas pipes and the rebars inside the concrete. Although several bands of IEEE 802.11ac waves with 160 MHz bandwidth can be combined to increase the range resolution as suggested by [9], the acquisition of such wide bands may be impossible in practice because the precious frequency resources and the penetration depth of 5 GHz WiFi signal may cause another problem.

Therefore, in order to apply WiFi signal into practical GPR applications, we propose to attach a passive sensor designed by SAW delay lines on the underground or inside-wall targets. In the sensor, a piezoelectric substrate converts an incoming electromagnetic signal into an acoustic signal whose velocity depends on the surrounding physical properties of the transducer [13]. The acoustic wave is reflected by mirrors patterned on the piezoelectric substrate back to the electrodes that convert the acoustic wave back to the electromagnetic wave, yielding an echo signal which has enough delay to be distinguished from the clutters. In this case, although the range resolution is not changed, the passive sensor can be effectively detected. Then, by simple calculations, the position of the target can be derived.

In order to verify the proposed method, several fundamental experiments are carried out. The configuration and the experiment setup including four measurement antennas are shown in Figs. 9 and 10, respectively. Since the surroundings of the experiment induce much stronger echoes than the response of the passive sensor, we also use ECA algorithm to reduce their influences. The range compression result obtained by the cross-correlation process is shown in Fig. 11, where the responses of the passive sensor can be well probed. Eight responses with delays ranging from 1 to 2.2 μs are detected, which are separated from the clutters that always have time delays in nanosecond scale. The 8-echoes are designed

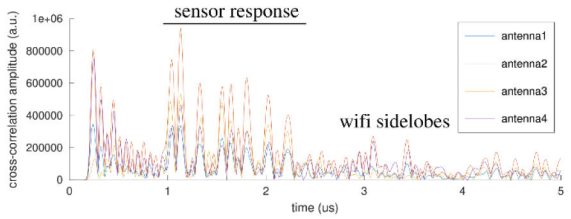

Fig. 11 *WiFi-based measurement of a passive sensor using IEEE 802.11n signal with 20 MHz bandwidth*

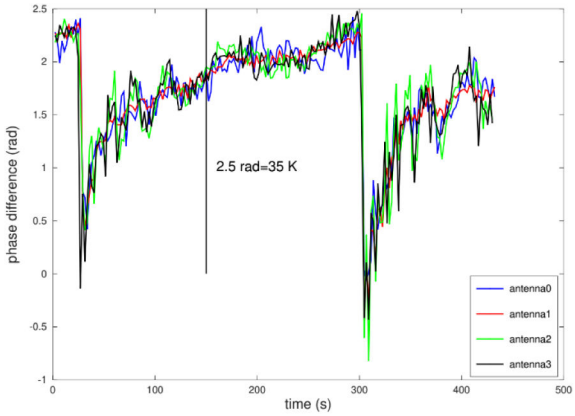

Fig. 12 *Temperature variation observed on the four antennas facing a SAW delay line cooled twice by a freezing spray at times 20 and 300 s*

Q4

as 8-bits allowing for identifying which structure is being observed.

In addition to tagging, fine acoustic velocity measurement allows for recovering the subsurface physical environmental property of the cooperative target. In this example, the strong temperature sensitivity $S = 60$ ppm/K of the lithium niobate piezoelectric substrate allows for detecting temperature variations. Indeed, a temperature variation d_T induces a phase variation $d\psi = 2\pi\tau f_0 S d_T$ with τ the delay difference between two echoes and $f_0 = 2.422$ GHz the central operating frequency. Echo time delay differences must be considered to get rid of the source to cooperative target delay dependence and measure a time delay only related to the acoustic velocity v since $\tau = D/v$ with D the geometric distance of the acoustic path, typically in the 3 mm range for a 1 µs delay. A one to one relation exists between phase and temperature as long as the temperature variation remains small enough to prevent 2π phase rotations, i.e. $\tau < 1/(S d_T f_0)$. In our case, considering a temperature range of 50 K, then two echoes separated by <138 ns must be selected. Such a condition is met by selecting any two adjacent pair of the echoes seen in the returned response of Fig. 11. Since the correlation is a linear process, the phase introduced by the acoustic delay line is also found on the cross-correlation output, allowing for the recovery of a temperature variation information as shown in Fig. 12.

Furthermore, the bistatic time delay plus direction of arrival (DOA) estimation of the SAW delay line is also conducted. Two case studies are presented, where the passive sensor is placed in different azimuth position but with the same bistatic range. In order to increase the angle estimation accuracy and resolution, the MUSIC algorithm [16] is applied in this case. As shown in Fig. 13, the position of the SAW delay line can be well detected.

4 Conclusion

We proposed and validated several WiFi-based passive bistatic radar imaging methods as the fundamental researches for GPR applications. The experimental results show that, combined with the passive cooperative sensor, it is possible to use WiFi as the transmitting source of GPR. Therefore, there is no need of frequency allocation, and it can save the system cost, increase the measurement flexibility, and reduce the electromagnetic pollution to the environment.

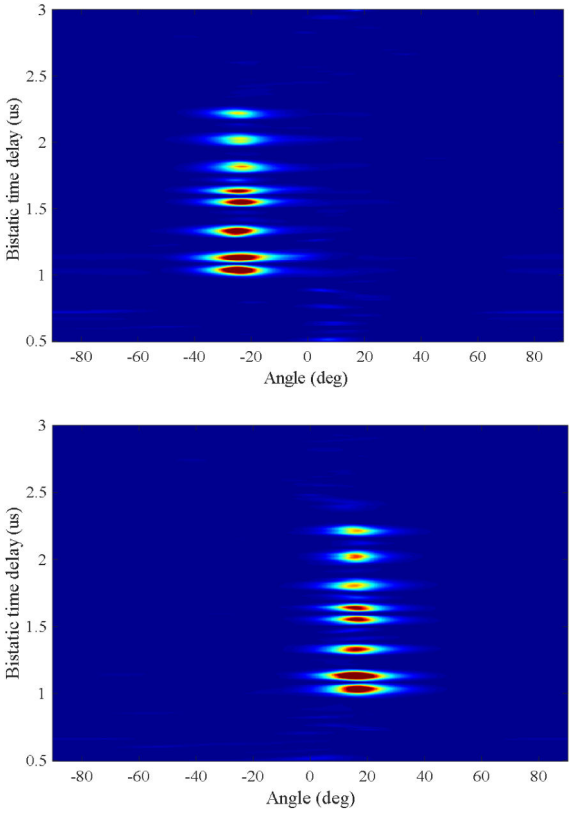

Fig. 13 *Bistatic time delay and angle estimation of the SAW delay line which is located at left (top) and right (bottom)*

5 Acknowledgments

This work was supported by JSPS Grant-in-Aid for Scientific Research (A) 26249058, OscillatorIMP and FIRST-TP grants from the French Projet d'Investissement d'Avenir (PIA), as well as Tohoku University through the funding of an invited scientist position for J.-M Friedt and a ROIS scholarship for Zhipeng Hu.

6 References

[1] Sato, M.: 'Introduction of the advanced ALIS: advanced landmine imaging system'. Detection and Sensing of Mines, Explosive Objects, and Obscured Targets XXIII, 2018, vol. 10628

Q1 [2] Economou, N., Benedetto, F., Bano, M., *et al.*: 'Advanced ground penetrating radar signal processing techniques', *Signal Process.*, 2017, **132**, pp. 197–200

[3] Feng, W., Friedt, J-M., Cherniak, G., *et al.*: 'Novel algorithm for high resolution passive radar imaging with ISDB-T digital TV signal'. Proc. IEEE Int. Geoscience and Remote Sensors Symp., Valencia, Spain, July 2018

[4] Feng, W., Friedt, J-M., Goavec-Merou, G., *et al.*: 'Passive RADAR measurement of acoustic delay lines used as passive sensors', *Electron. Lett.*, 2018, under review

Q2 [5] Chetty, K., Smith, G.E., Woodbridge, K.: 'Through-the-wall sensing of personnel using passive bistatic WiFi radar at standoff distances', *IEEE Trans. Geosci. Remote Sens.*, 2012, **50**, (4), pp. 1218–1226

[6] Colone, F., Woodbridge, K., Guo, H., *et al.*: 'Ambiguity function analysis of wireless LAN transmissions for passive radar', *IEEE Trans. Aerosp. Electron. Syst.*, 2011, **47**, (1), pp. 240–264

[7] Colone, F., Falcone, P., Bongioanni, C., *et al.*: 'Wifi-based passive bistatic radar: data processing schemes and experimental results', *IEEE Trans. Aerosp. Electron. Syst.*, 2012, **48**, (2), pp. 1061–1079

[8] Huang, D., Nandakumar, R., Gollakota, S.: 'Feasibility and limits of Wi-Fi imaging'. Proc. ACM Conf. Embedded Netw. Sensor Syst., 2014, pp. 266–279

[9] Shi, J., Liu, Y., Liu, W., *et al.*: 'High-resolution synthetic aperture radar based on the IEEE 802.11 protocol', *Electron. Lett.*, 2015, **51**, (22), pp. 1815–1817

[10] Lamothe, M., Plessky, V., Friedt, J.-M., *et al.*: 'Ultra-wideband SAW sensors and tags', *Electron. Lett.*, 2013, **49**, (24), pp. 1576–1577

Q3 [11] Ding, Z., Wang, Z., Lin, S., *et al.*: 'Local fringe frequency estimation based on multifrequency InSAR for phase-noise reduction in highly sloped terrain', *IEEE Geosci. Remote Sens. Lett.*, 2017, **14**, (9), pp. 1527–1531

[12] Ding, Z., Guo, Y., Gao, W., *et al.*: 'A range grating lobes suppression method for stepped-frequency SAR imagery', *IEEE J. Sel. Top. Appl. Earth Observ. Remote Sens.*, 2016, **9**, (12), pp. 5677–5687

[13] Friedt, J.-M., Martin, G., Goavec-Mérou, G., *et al.*: 'Acoustic transducers as passive cooperative targets for wireless sensing of the sub-surface world: challenges of probing with ground penetrating RADAR', *Sensors*, 2018, **18**, (1), p. 246

[14] Colone, F., Cardinali, R., Lombardo, P.: 'Cancellation of clutter and multipath in passive radar using a sequential approach'. Proc. of IEEE Int. Conf. on Radar, 2006

[15] Feng, W., Yi, L., Sato, M.: 'Near range radar imaging based on block sparsity and cross-correlation fusion algorithm', *IEEE J. Sel. Top. Appl. Earth Observ. Remote Sens.*, 2018, **11**, (6), pp. 2079–2089

[16] Odendaal, J.W., Barnard, E., Pistorius, C.W.I.: 'Two-dimensional superresolution radar imaging using the MUSIC algorithm', *IEEE Trans. Antennas Propag.*, 1994, **42**, (10), pp. 1386–1391

JOE20190209

Author Queries

Q Please make sure the supplied images are correct for both online (colour) and print (black and white). If changes are required please supply corrected source files along with any other corrections needed for the paper.
Q1 Please provide place of conference for Refs. [1, 8, 14].
Q2 Please provide volume number, page range for Ref. [4].
Q3 Please note as reference number [10] is appearing twice in the reference list. It has been renumbered in the list and text citations. Please confirm.
Q4 Please check the edits made to the Figure caption 12 "Temperature variation...".